

Contemporary deformation in the Yakima fold and thrust belt estimated with GPS

Robert McCaffrey,¹ Robert W. King,² Ray E. Wells,³ Matthew Lancaster¹ and M. Meghan Miller⁴

¹Portland State University, Portland, OR, USA. Email: mccaffr@gmail.com

²Massachusetts Institute of Technology, Cambridge, MA, USA

³US Geological Survey, Menlo Park, CA, USA

⁴UNAVCO, Boulder, CO, USA

Accepted 2016 July 4. Received 2016 July 2; in original form 2016 January 13

SUMMARY

Geodetic, geologic and palaeomagnetic data reveal that Oregon (western USA) rotates clockwise at 0.3 to $1.0^\circ \text{ Ma}^{-1}$ (relative to North America) about an axis near the Idaho–Oregon–Washington border, while northeast Washington is relatively fixed. This rotation has been going on for at least 15 Ma. The Yakima fold and thrust belt (YFTB) forms the boundary between northern Oregon and central Washington where convergence of the clockwise-rotating Oregon block is apparently accommodated. North–south shortening across the YFTB has been thought to occur in a fan-like manner, increasing in rate to the west. We obtained high-accuracy, high-density geodetic GPS measurements in 2012–2014 that are used with earlier GPS measurements from the 1990s to characterize YFTB kinematics. The new results show that the deformation associated with the YFTB starts at the Blue Mountains Anticline in northern Oregon and extends north beyond the Frenchman Hills in Washington, past the epicentre of the 1872 M_w 7.0 Entiat earthquake to 49°N . The north–south strain rate across the region is 2 to $3 \times 10^{-9} \text{ yr}^{-1}$ between the volcanic arc and the eastern edge of the YFTB (241.0°E); east of there it drops to about 10^{-9} yr^{-1} . At the eastern boundary of the YFTB, faults and earthquake activity are truncated by a north-trending, narrow zone of deformation that runs along the Pasco Basin and Moses Lake regions near 240.9°E . This zone, abutting the Department of Energy Hanford Nuclear Reservation, accommodates about 0.5 mm yr^{-1} of east to northeast shortening. A similar zone of N-trending transpression is seen along 239.9°E where there is a change in the strike of the Yakima folds. The modern deformation of the YFTB is about 600 km wide from south to north and internally may be controlled by pre-existing crustal structure.

Key words: Space geodetic surveys; Plate motions; Continental neotectonics; Continental tectonics: compressional; North America.

1 INTRODUCTION

The Yakima fold and thrust belt (YFTB) is an actively deforming series of faults and folds in northern Oregon and south-central Washington in the northwestern United States (Fig. 1). Through it runs the Olympic-Wallowa Lineament (OWL; Raisz 1945), an alignment of topographic features that extends from eastern Oregon into the Puget Sound region of Washington. The YFTB forms the boundary between the clockwise-rotating Oregon block (Fig. 2) and eastern Washington, nominally attached to the North American Plate (Wells *et al.* 1998; McCaffrey *et al.* 2000, 2013). The location of the relative rotation pole between Oregon and Eastern Washington near the southeast edge of the YFTB suggests that the shortening rate across the belt may increase to the west, in the manner of a fan closing.

Recent work by Blakely *et al.* (2011) suggests that some faults of the YFTB can be traced northwestward through the Cascade volcanic arc possibly connecting to faults in the Puget Lowlands where Seattle is located. While we have suggested earlier, based on GPS observations, that the regions are kinematically linked through the accommodation of Oregon's rotation (McCaffrey *et al.* 2000), the possible continuation of the fault planes through the arc has important implications for hazards – simply put, longer faults can produce larger magnitude and longer-duration earthquakes. We present a new high-density, high-accuracy GPS velocity field for the YFTB and surroundings based on recent (2012–2014) re-occupations of ~60 geodetic monuments that had been previously measured (most of them in 2001 or earlier) and on updated velocities from many continuous GPS stations.

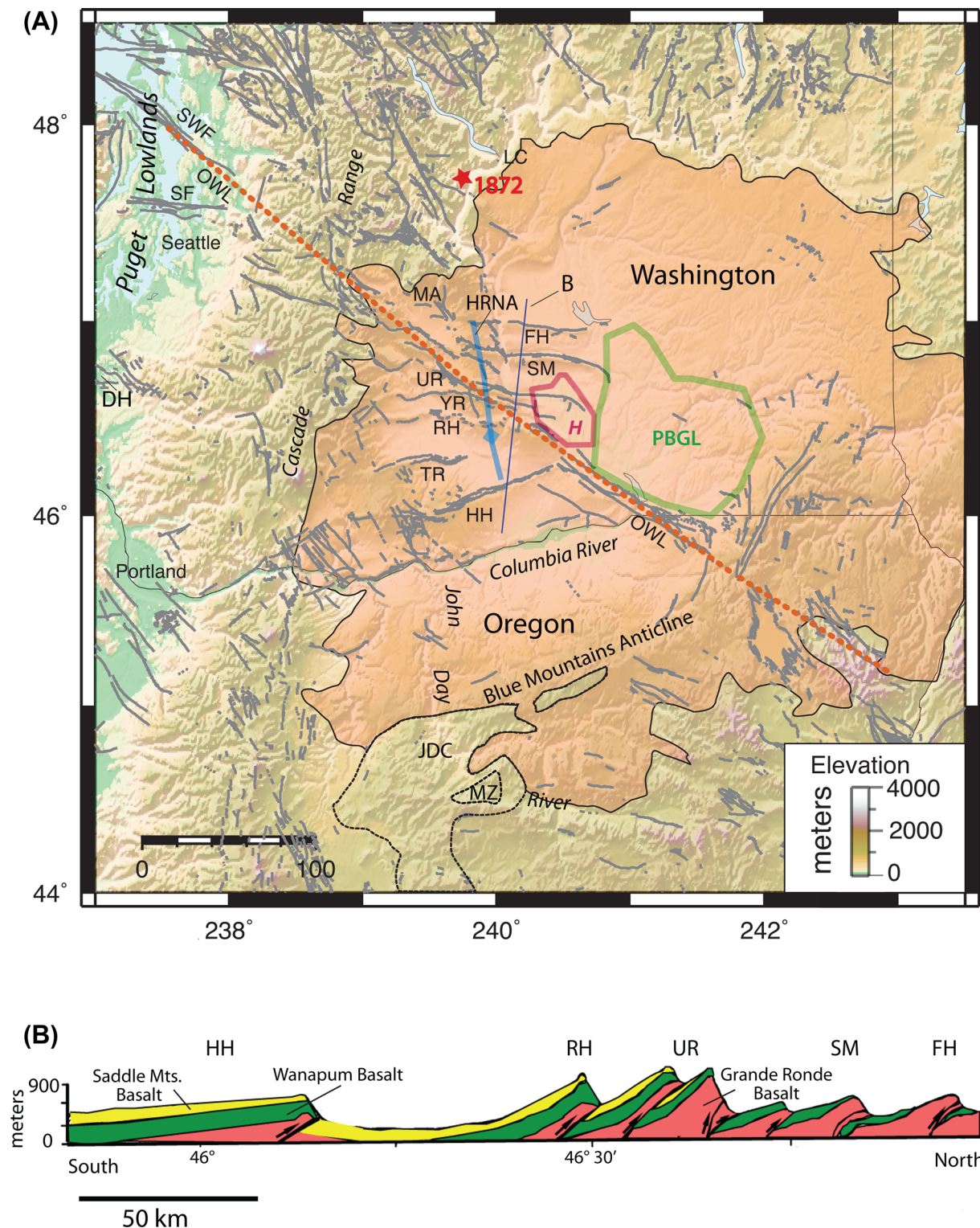


Figure 1. (A) Location of the Yakima fold and thrust belt (YFTB), Oregon and Washington. Faults (grey lines) from the U.S.G.S. Quaternary fault database (<http://earthquake.usgs.gov/hazards/qfaults>). Major YFTB structures labelled; FH: Frenchman Hills, SM: Saddle Mountains, UR: Umtanum Ridge, RH: Rattlesnake Hills, TR: Toppenish Ridge, HH: Horse Heaven Ridge, MA: Manastash Anticline, HRNA: Hog Ranch–Naneum Anticline (blue line), PBGL: Pasco Basin gravity low (green polygon; Blakely *et al.* 2014). H: Hanford nuclear facility outlined in red. Brown dashed line is Olympic–Wallowa Lineament (OWL). ‘1872’ shows the location of the 1872 earthquake (Sherrod *et al.* 2015) near Lake Chelan (LC). Other features: SWF: South Whidbey fault, SF: Seattle fault, DH: Doty Hills, JDC: Palaeogene John Day and Clarno Formations over Mesozoic rocks (MZ) exposed in Blue Mountains uplift. Line B is the location of the schematic cross-section in (B). Light orange region shows extent of Columbia River Basalt Group. (B) Schematic cross-section along a south-to-north line taken from Reidel *et al.* (1989). The colouring represents separate basalt units (pink: Grande Ronde; green: Wanapum; yellow: Saddle Mountains).

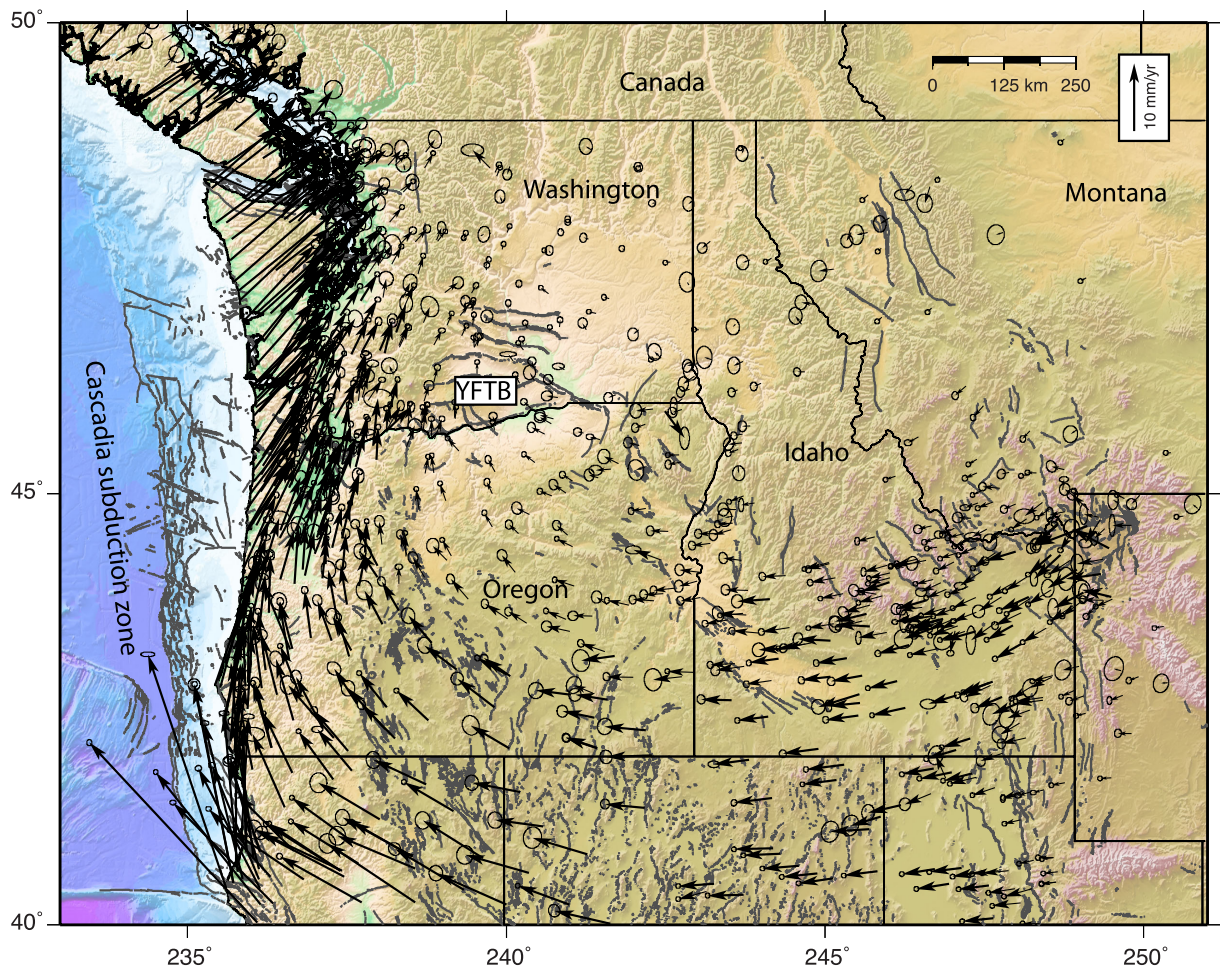


Figure 2. Velocity field of the Pacific Northwest relative to North America, as of 2015 February 27. Error ellipses are at 70 per cent confidence level. YFTB: Yakima fold and thrust belt. Fault lineations are shown as grey lines.

2 THE YAKIMA FOLD AND THRUST BELT

The YFTB is located east of the Cascade volcanic arc of Washington and Oregon. The folds and faults of the YFTB deform Columbia River Basalt Group (CRBG) flows as well as Miocene to Pleistocene sedimentary rocks that overlie them. The deforming region consists of asymmetrical, ridge-forming anticlines labelled on Fig. 1, separated by valleys 10–20 km across. The folds appear to be underlain by thrusts, also shown in Fig. 1 (Reidel *et al.* 1989, 1994, 2013; Yeats 2011). The Yakima and Columbia Rivers (CRs) cut the folds and appear to be antecedent to uplift (Waters 1955). Folding may have initiated prior to eruption of the CRBG, as gravity data indicate asymmetric basement highs beneath the folds that are greater than the amplitude of folding in the CRBG (Blakely *et al.* 2011). Folding continued during emplacement of the CRBG and following its eruption (Reidel *et al.* 1994).

Within the YFTB, several structures have revealed evidence of Holocene deformation, for example the Saddle Mountains, Umatum Ridge, Toppenish Ridge and Manastash Anticline structures (Fig. 1; Campbell & Bentley 1981; Reidel *et al.* 1994; West *et al.* 1996; Ladinsky *et al.* 2010; Blakely *et al.* 2011). According to Reidel *et al.* (1994), over 10.5 Myr the folds have accommodated at least 15–25 km of shortening and faulting along an N–S profile at longitude 240°E. A possible connection can be made of faults of the YFTB through the Cascade arc to the Southern Whidbey Island

fault within the highly populated Puget Lowlands region (Blakely *et al.* 2011; Fig. 1). Such a system would be long enough to produce a magnitude 7 or larger earthquake. The YFTB is a concern for seismic hazards assessment due to the location of many critical facilities, such as dams and the Department of Energy Hanford Site, within its borders (Fig. 1).

The folds and faults of the YFTB are not parallel but instead fall into three groups of orientations. North of the OWL and east of the CR the Saddle Mountain and Frenchman Hills trend approximately E–W while their westward extensions, west of the CR, have a more ESE trend. South of the OWL, the folds of the Yakima Ridge and Horse Heaven Hills trend ENE. Pratt (2012) suggests that the geometry of the folds is a remnant of earlier strike-slip faulting on the OWL that decreased in amplitude westward, i.e., that they formed around the edge of a shear crack tip. Reidel *et al.* (2013) give evidence that there has been no strike-slip on the OWL since emplacement of the Grand Ronde Basalt at ~15 Ma and that changes in the fold orientations arise from pre-existing basement structure. The current GPS-derived velocity field shows no indications that any strike-slip on the OWL occurs today (McCaffrey *et al.* 2013). As we show, some of the changes in fault orientation may arise from active shear on N–S planes.

The YFTB has distributed earthquake activity that appears to be elevated relative to regions to the south and east but considerably less than in the Puget Sound region to the northwest (Fig. 3; Ludwin

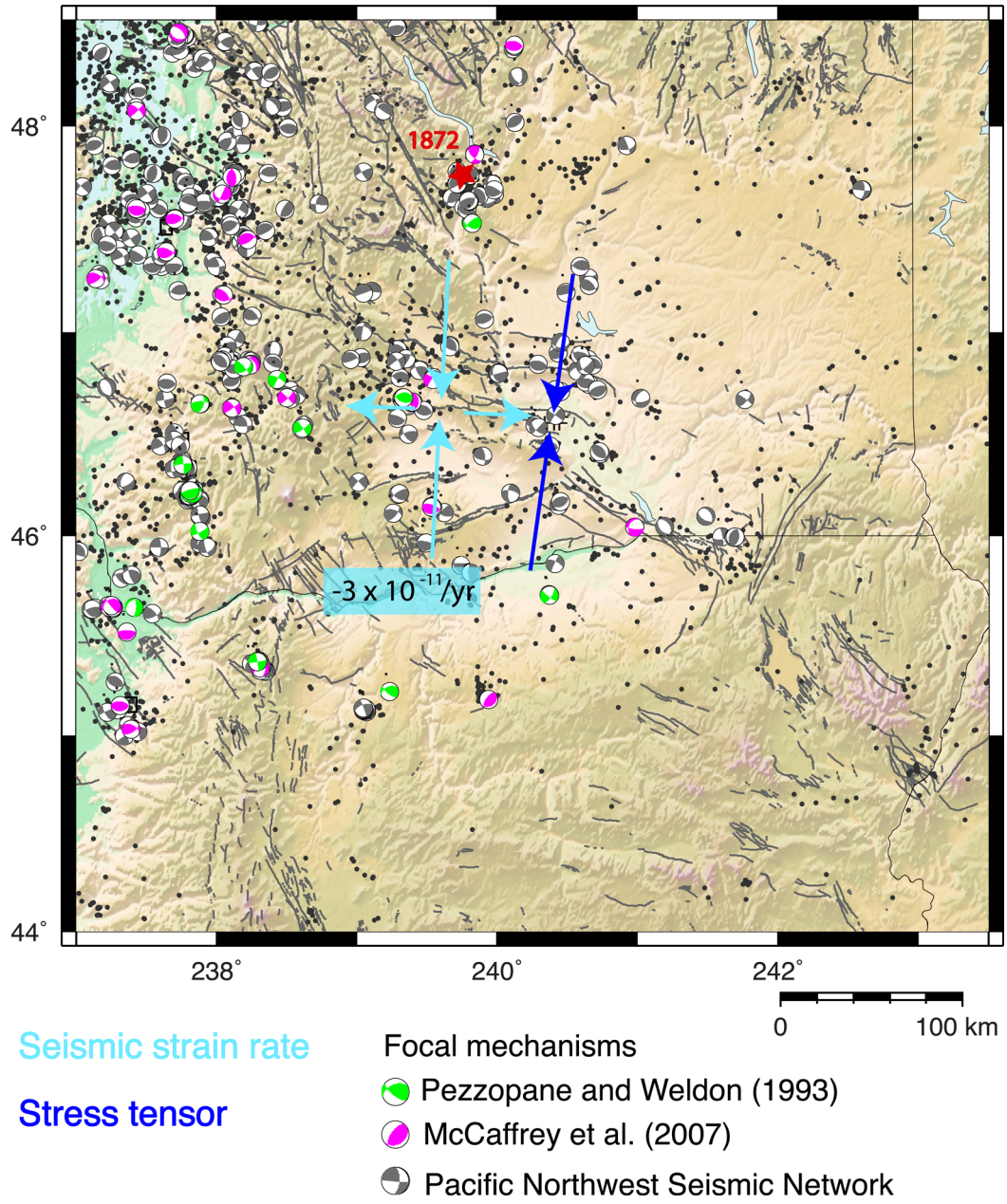


Figure 3. Seismicity of the Yakima region. Dots: epicentres taken from ANSS from 1980–April 2011, where depth is less than 40, magnitude greater than 2; representative focal mechanisms shown. Light blue arrows show the principal strain rates derived from earthquake moment tensors. Dark blue arrows show the direction of maximum compressive stress derived from the same earthquakes.

et al. 1991; Gomberg *et al.* 2012). Earthquakes have occurred in several swarms that vary in depth. Most seismicity is shallow, less than 4 km, but some earthquakes are as deep as 25–30 km. Focal mechanisms show predominantly reverse motion on E- and SE-striking faults, consistent with orientation of Yakima folds, though strike-slip events are observed as well, suggesting that strain is partitioned. Gomberg *et al.* (2012) suggest that seismicity in the YFTB is more related to hydrologic changes in the CRBG than to tectonic deformation. Inversions of earthquake focal mechanisms for an average stress tensor by McCaffrey *et al.* (2013) suggest that the trend of the most compressive stress is between 4° and 12° east of north (Fig. 3; dark blue arrows) with a plunge of 3°–13°, thereby largely revealing ~N–S contraction and vertical extension (crustal thickening), consistent with the interpretations of the YFTB struc-

tures and a tectonic origin for the earthquakes. From the same set of earthquakes, they also performed a Kostrov (1974) seismic moment summation to estimate the strain rate tensor (elastic thickness of 10 km, rigidity of 40 GPa) to be $-0.03 \times 10^{-9} \text{ yr}^{-1}$ at N3°E (Fig. 3; light blue arrows), which is ~2 orders of magnitude lower than the modern geodetic strain rate. This difference may indicate that the strain in the YFTB is largely aseismic or that there is considerable moment deficit rate that might be leading to a large earthquake. The analysis did not include the 1872 $M \sim 7$ Entiat earthquake that has now been reliably located at the northern edge of the YFTB (Sherrod *et al.* 2015). Including the seismic moment from that event would roughly equalize the geodetic and seismic strain rates (McCaffrey *et al.* 2013) though large uncertainties exist in all such calculations.

Savage *et al.* (1981, 1991) reported on electronic line-length measurements from a network of 19 markers in the Hanford region (Fig. 1) measured from 1972 to 1983. They concluded that there was no resolvable strain rate during that time but their uncertainties were large, on the order of $10 \text{ nstrain yr}^{-1}$ ($1 \text{ nstrain} = 10^{-9}$), which is larger than the average strain rate we estimate for the entire YFTB from more recent GPS observations (McCaffrey *et al.* 2013).

3 GLOBAL POSITIONING SYSTEM MEASUREMENTS

3.1 Observations and analysis

In 2012 and 2013 we re-occupied about 60 survey-mode GPS (sGPS) sites in and around the YFTB (Supporting Information Fig. S1) to provide velocities based on 10 or more years at most sites. Each site was occupied for at least 16 hours. To further densify the velocity field, we also processed the data acquired between 2004 and 2014 from 20 to 50 PANGA sites, and we combined our estimates and covariances with similar solution files from the PBO GAMIT processing at New Mexico Tech (M. H. Murray, private communication; <ftp://data-out.unavco.org/pub/products/sinex/>). Details of the data used are given in the Supporting Information.

We analysed the collected GPS phase data using the GAMIT/GLOBK software (Herring *et al.* 2010) following the approach described in section 2.2 of McCaffrey *et al.* (2007). The velocities were determined relative to stable North America (without correction for global isostatic adjustment) by estimating a six-parameter transformation (three translation rates and three rotation rates) while minimizing the adjustments from the PBO velocity field of 227 continuous stations in North America (ftp://data-out.unavco.org/pub/products/position/gage_gps.nam08.txt). Uncertainties in the velocities were estimated in the manner described by McCaffrey *et al.* (2007) and detailed in the Supporting Information.

We estimate vertical rates of motion at all sites but they are not used here due to relatively large uncertainties and generally slow vertical tectonic rates. We do not apply corrections to the velocity field as others have done (e.g., Puskas & Smith 2009; Pollitz *et al.* 2010) to account for mantle relaxation from past earthquakes. As we discuss in detail in McCaffrey *et al.* (2013), the N–S contraction we observe across the YFTB is opposite in sign from the expected post-seismic deformation expected from the Cascadia subduction zone (Pollitz *et al.* 2010), the only fault long enough to produce the long wavelengths we see in the GPS. We make corrections in the GPS time series for earthquake offsets but not for slow-slip events from the Cascadia subduction zone.

3.2 Uncertainties in GPS velocities

Our error model incorporates both random (white noise) and time-correlated noise calibrated to obtain velocity uncertainties consistent with the confidence levels of their error ellipses, as described by McCaffrey *et al.* (2007). To account for the random noise, we add quadratically to each position estimate an uncertainty (typically $0.5\text{--}1.5 \text{ mm}$) necessary to make the normalized scatter of the time series consistent with the median for all of the stations. To account for the correlated noise, we use the First-Order Gauss–Markov Extrapolation algorithm of Herring (2004), described further in McCaffrey *et al.* (2013). In our current analysis, we estimate the process noise for the north and east components for each cGPS station from their time series; for the sGPS stations we used the median value

($\sim 0.5 \text{ mm sqrt-yr}^{-1}$) obtained for the cGPS stations. As in our previous papers, we validated our error model by comparing the normalized scatter of velocity residuals in a well-modelled, smoothly deforming region with the scatter predicted by a Gaussian distribution (McCaffrey *et al.* 2007, 2013; Supporting Information Fig. S2). For the current analysis, the normalized rms (nrms) of the GPS residuals is 1.1 and the weighted rms 0.3 mm yr^{-1} .

4 RESULTS

4.1 Regional velocity field

Fig. 2 shows the regional velocity field we have generated through February 2015 (solution PNW150227 relative to North America; Supporting Information Table S1). The large-scale clockwise rotation of Oregon, Nevada and the Snake River Plain is clear and is discussed in our earlier papers (McCaffrey *et al.* 2000, 2007, 2013). Of primary interest here, the rotation appears to end in the vicinity of the YFTB in southwestern Washington. The drop in velocity across the region between central Oregon and central Washington from south to north is about $3\text{--}4 \text{ mm yr}^{-1}$ at the west end of the region (near the Cascade Range, Fig. 1) and near zero at its eastern end. The other large strain signal present is the easterly contraction near the coast due to subduction zone locking. While the deformation rate across the YFTB has been estimated from geologic studies of active faulting, the active deformation can be estimated in detail from our GPS velocities.

4.2 YFTB velocities relative to Washington

Fig. 4(b) shows the GPS velocities in an eastern Washington reference frame, determined by minimizing the motion of the sites east of 241°E . In this view there are two visibly abrupt changes in the velocities (denoted by blue dashed lines in Fig. 4b); one along approximate longitude 239.9°E and the other along 240.9°E . West of 239.9°E the vectors are generally pointed NE at about $1\text{--}2 \text{ mm yr}^{-1}$. Between 239.9° and 240.9° they are much smaller but still systematically point \sim eastward while east of 241°E they are scattered about zero (as defined by this reference frame). Crossing the western of the two identified N–S trends, the faults in the northern half of the YFTB change from a westerly strike (to the east) to more WNW (west of the trendline). This change in strike of the faults suggests right-lateral shear along the N–S trend, consistent with the GPS vectors. The change in velocities along the eastern of the two trends also indicates slow ENE convergence across this boundary, which is parallel to the CR and near the eastern boundary of the Hanford Site (Fig. 4a). This trend also marks the easternmost edge of the most pronounced seismicity of the YFTB and near the eastern truncation of the YFTB faults (Figs 3 and 4c). While the folds appear to continue east of this zone (Reidel *et al.* 2013) their amplitudes decrease significantly and go through a dextral bend similar to that of the western trend. Using the sites between 46°N and 47.4°N , the average velocities, written as (East, North), relative to the region east of 241°E , of the western group is $(1.1 \pm 0.1, 0.6 \pm 0.2) \text{ mm yr}^{-1}$ (average of 20 sites) and the central block moves at $(0.5 \pm 0.1, 0.2 \pm 0.1) \text{ mm yr}^{-1}$ (average of 20 sites; Fig. 4c). These velocities indicate that the relative motion across both boundaries is about 0.5 mm yr^{-1} of shortening and $0.2\text{--}0.3 \text{ mm yr}^{-1}$ of right-lateral shear. The strain across both of these boundaries is aligned with Cascadia subduction strain, though we argue later that features along both zones suggest they are revealing permanent deformation.

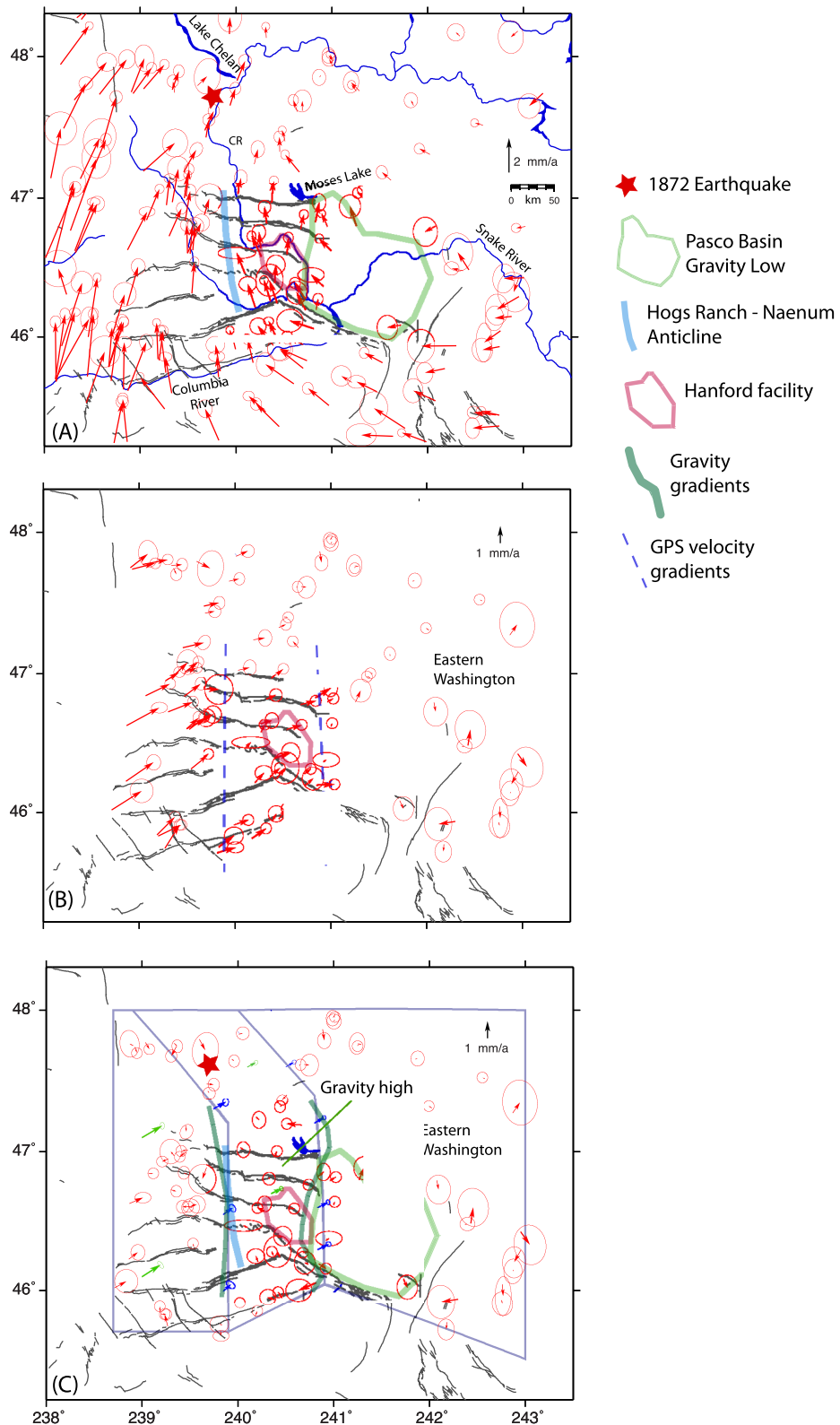


Figure 4. (A) Observed GPS velocities within the YFTB area, relative to North America. Only those with uncertainties of less than 0.8 mm yr^{-1} are shown (error ellipses are at 70 per cent confidence level). Fault lineations are shown as grey lines and rivers/lakes as blue. Hog Ranch–Naenum Anticline described by Reidel *et al.* (2013). Pasco Basin gravity low from Blakely *et al.* (2014). (B) GPS velocities relative to eastern Washington. (C) Residual velocities (red) after removing rotation of western and central YFTB relative to eastern Washington. Blue vectors show relative velocities across blue boundaries and green vectors are motions relative to eastern Washington. Green curves show approximate outline of gravity high described by Lamb *et al.* (2015).

4.3 Strain rates

To estimate the regional geodetic deformation, we take a region encompassing the YFTB and estimate the spin rate and uniform horizontal strain rate from the 52 GPS velocities within it. From the GPS velocities in the North American reference frame, the vertical

axis rotation rate is $-0.43 \pm 0.02^\circ \text{ Ma}^{-1}$ with a pole to the east (Figs 5a and b). This spin rate is similar to the rate measured using palaeomagnetic methods for the 12–15 Ma CRBG, suggesting that the rotation is long-lived (McCaffrey *et al.* 2007; Wells & McCaffrey 2013). The average strain rate tensor has its maximum contraction

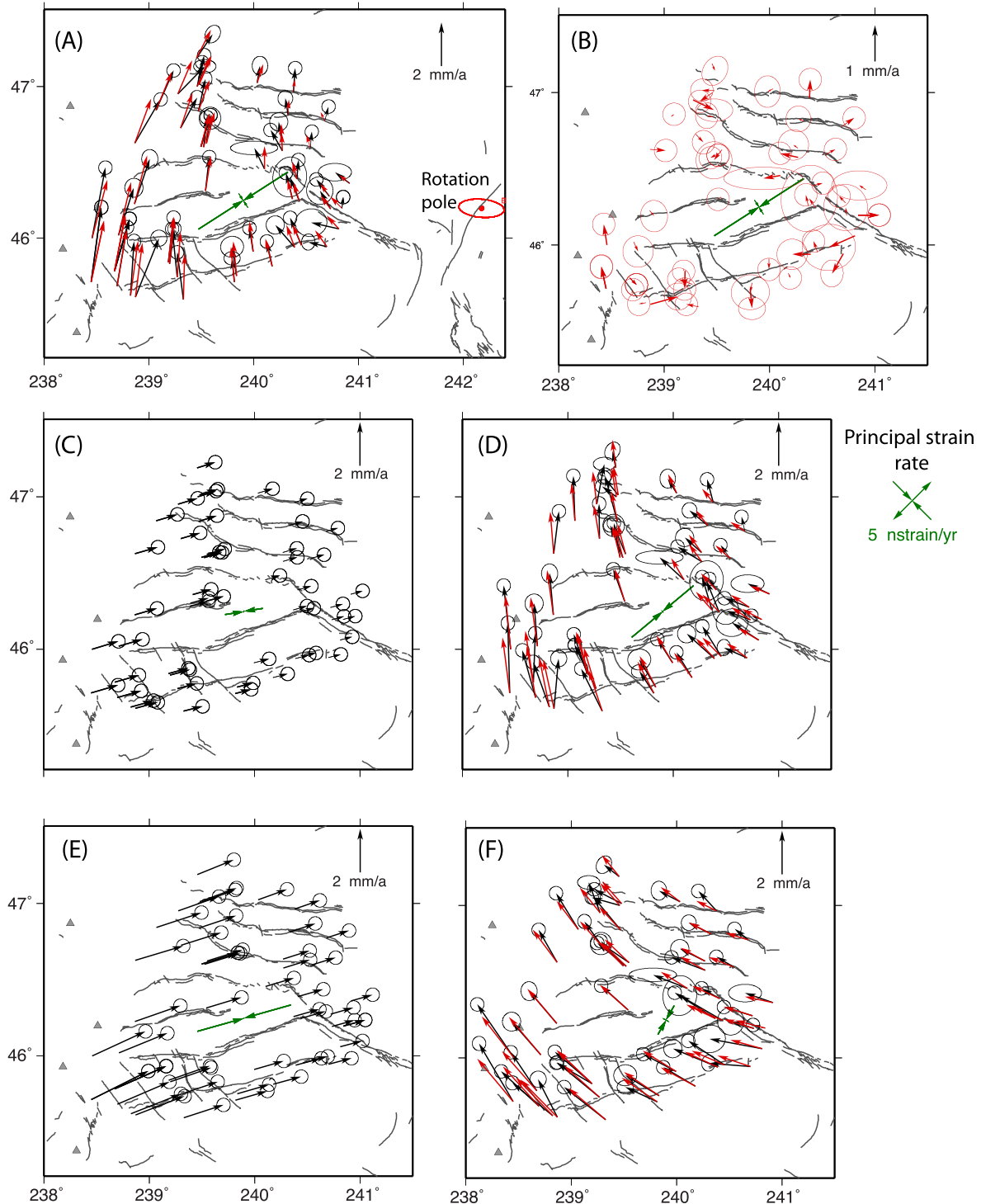


Figure 5. (A) Observed (black) and calculated (red) velocities within the YFTB, relative to North America. Fault lineations are shown as grey lines. A rotation pole (shown at eastern edge with its error ellipse) and uniform horizontal strain rate were fit to the velocities. Green arrows show principal strain rate; scale is same for all panels. (B) Velocity residuals for calculation in panel (A). (C) Predicted velocities and strain rate from locking model where locking is Gaussian and largely offshore (Fig. S3a). (D) Calculated strain rate for velocities corrected for locking strain rate in (C). (E) Predicted velocities and strain rate from locking model where locking is represented by a grid (Fig. S3b). (F) Calculated strain rate for velocities corrected for locking strain rate in (E).

rate of -9.8 ± 0.6 nstrain yr^{-1} (contraction is negative) in an NE direction ($57^\circ \pm 3^\circ$ east of north). Part of this strain rate is due to the ~E–W contraction noted above, N–S motion of Oregon into Washington and part is due to elastic strain from locking at Cascadia. Evidence that Cascadia locking produces strain across the YFTB is the presence of westward deflections of cGPS sites within the YFTB during Cascadia slow-slip events (Supporting Information Fig. S3).

To bracket the impact of the Cascadia subduction zone elastic component we take the predicted locking strain-rate velocities from two Cascadia locking models (Supporting Information Figs S4a and b) that may represent minimum and maximum locking distributions that satisfy both the GPS and coastal levelling data (see McCaffrey *et al.* 2013). One model assumes a Gaussian distribution of locking with depth, which places most of the locking offshore. This locking model predicts a small impact on the YFTB velocities (Fig. 5c) resulting in a strain rate of -3.5 nstrain yr^{-1} at an azimuth of 081° due to the locking. Subtracting these velocities from the observed and estimating rotation and strain rate as above gives a strain rate of -7.4 nstrain yr^{-1} at azimuth of 050° (Fig. 5d). An alternative locking model is estimated by allowing Cascadia locking to vary on a grid on the plate interface. This model matches more of the on-land strain rates with plate interface locking than does the Gaussian model and predicts a larger locking-induced strain rate in the YFTB; -8.9 nstrain yr^{-1} at 074° azimuth (Fig. 5e). Subtracting these velocities from the observed velocities results in a strain rate of -3.1 nstrain yr^{-1} at 030° azimuth (Fig. 5f). In both cases the corrected velocities give a spin rate of $-0.39^\circ \text{ Ma}^{-1}$, nearly equal to the uncorrected spin rate of $-0.43^\circ \text{ Ma}^{-1}$.

The YFTB geodetic contraction direction of $N30^\circ\text{E}$ obtained by the larger locking correction is much closer to the stress and strain directions inferred from earthquakes ($N3^\circ\text{E}$ to $N12^\circ\text{E}$; Fig. 3 and McCaffrey *et al.* 2013). It is oblique to the E–W trends of some faults and folds of the belt but more normal to the NW trends of others. The maximum contraction direction from GPS is similar to the direction of shortening inferred from InSAR line-of-sight changes for the 2009 Wooded Island swarm (Wicks *et al.* 2011). The contraction rate derived from summing earthquake moment tensors is -0.03 nstrain yr^{-1} (McCaffrey *et al.* 2013), which is 100 times smaller than the corrected geodetic rate (-3.1 nstrain yr^{-1}) in approximately the same direction. Wicks *et al.* (2011) showed that about 90 per cent of the geodetic moment in the Wooded Island swarm was aseismic, which, if generally true, explains some of the strain rate discrepancy, while future (or past) large earthquakes may also account for the moment rate deficit. The 1872 earthquake near Lake Chelan, with a magnitude of 6.5 to 7.0 (Bakun *et al.* 2002) appears to be due to ~N–S shortening (Sherrod *et al.* 2015) and adds a significant portion to the observed YFTB seismic moment budget.

The discrepancy between the seismic direction of shortening and the geodetic direction may indicate a lack of seismicity associated with the apparent E–W shortening on the two N–S zones of transpression identified with GPS. If these are both permanent deformation features, they are lacking in related seismicity and may be either aseismic or in the pre-seismic stage.

4.4 South-to-north GPS profiles

The strain rates estimated above are averages over a broad region within which there are clear spatial variations. To examine the GPS results in more detail as they pertain to local structures we present

a series of south-to-north profiles of the north component of the GPS velocities; the slopes of these lines give the normal strain rates in the north direction ε_{NN} (negative slopes represent contraction). The ε_{NN} component will not contain any bias due to rotation. Since the elastic strain rates from the subduction zone are largely E–W compression, their impact on ε_{NN} is small. (Based on the grid locking model, for the forearc the expected N–S strain rate from locking is ~ 2.2 nstrain yr^{-1} of extension, while in the backarc it is < 0.5 nstrain yr^{-1} of contraction.) Fig. 6 shows south-to-north profiles of the north components of velocities every 0.5° of longitude from 236.5°E to 242.0°E . GPS points plotted along each profile are those within 25 km of the specified line of longitude (projections of points onto a line leads to some of the scatter in the profiles). West of the arc (which falls around 238.2°E), the average strain rates are near zero from 43°N to around 46.7°N where there is a 1–2 mm yr^{-1} drop across the Willapa and Doty Faults. North of the Doty Fault there is strong contraction, which seems to be localized in part at the Seattle Fault (SF). Forearc deformation will be the topic of a separate paper, as it requires detailed assessment of the Cascadia locking. (These profiles are plotted in a more traditional format in the Supporting Information, along with fits for estimated uniform and spatially varying strain rates.)

East of the arc (near 238°E ; Fig. 6), the first change in velocities seen (going from bottom to top in the figure, or south to north geographically) in the profiles is at about 44°N on profile 238.5°E . This drop in velocity continues in the profiles to the east (in 239.0°E through 240.5°E) but also moves north. This contractional velocity gradient coincides with the axis of the Blue Mountains Anticline (BMA; pink curve in Fig. 6). The Blue Mountains uplift may act like a large Yakima fold, with faults along its northern flank, possibly along the John Day River where it flows west, eroding into the uplifted, Mesozoic rocks exposed in the core (Fig. 1). The Blue Mountains represent the southernmost transition from ~E–W extension of the Basin and Range to N–S compression associated with the greater YFTB. A few Basin and Range faults cut up into the Blue Mountains but do not make it through, except in the Clearwater embayment along the Idaho border area.

The near-vertical dashed lines on the figure have a slope of -2 nstrain yr^{-1} and seem to fit the slopes for most of the profiles north of the BMA. Between the BMA and the CR there appears to be a small negative gradient in the velocities, indicating contraction, though the short distance and scatter in GPS velocities preclude a clear determination of the rate. Across the YFTB (from the CR to 47°N , the Frenchman Hills) again slight N–S contraction is evident. However, north of the YFTB (Fig. 6), the gradient in most of the profiles (238.5° to 241.0°E) continues to at least 49°N and possibly farther north. The northern gradient coincides in latitude with the high strain rates and faulting through the Seattle region. It also includes the epicentre of the 1872 earthquake.

Fig. 6 gives the average strain rates ε_{NN} along each profile, using the entire profile (43°N to 50°N ; strain rates listed at top). West of the arc the average strain rates are consistently around 5 nstrain yr^{-1} (ranging from 4.8 to 5.3 nstrain yr^{-1}) though the deformation is located only north of about 47°N (see Supporting Information Fig. S6). From the arc ($\sim 238^\circ\text{E}$) to about 240.5°E the strain rates are about half of that, ranging from 2.4 to 2.9 nstrain yr^{-1} , and uniform along nearly the entire profile. From 241.0°E to the east they halve again, ranging from 1.1 to 1.5 nstrain yr^{-1} . (As noted above, based on our models, these differences do not arise from the Cascadia locking.) Such a pattern of eastward decreasing strain rates are consistent with a clockwise rotation of Oregon but the abrupt changes at the arc and at 241°E indicate that small amounts of

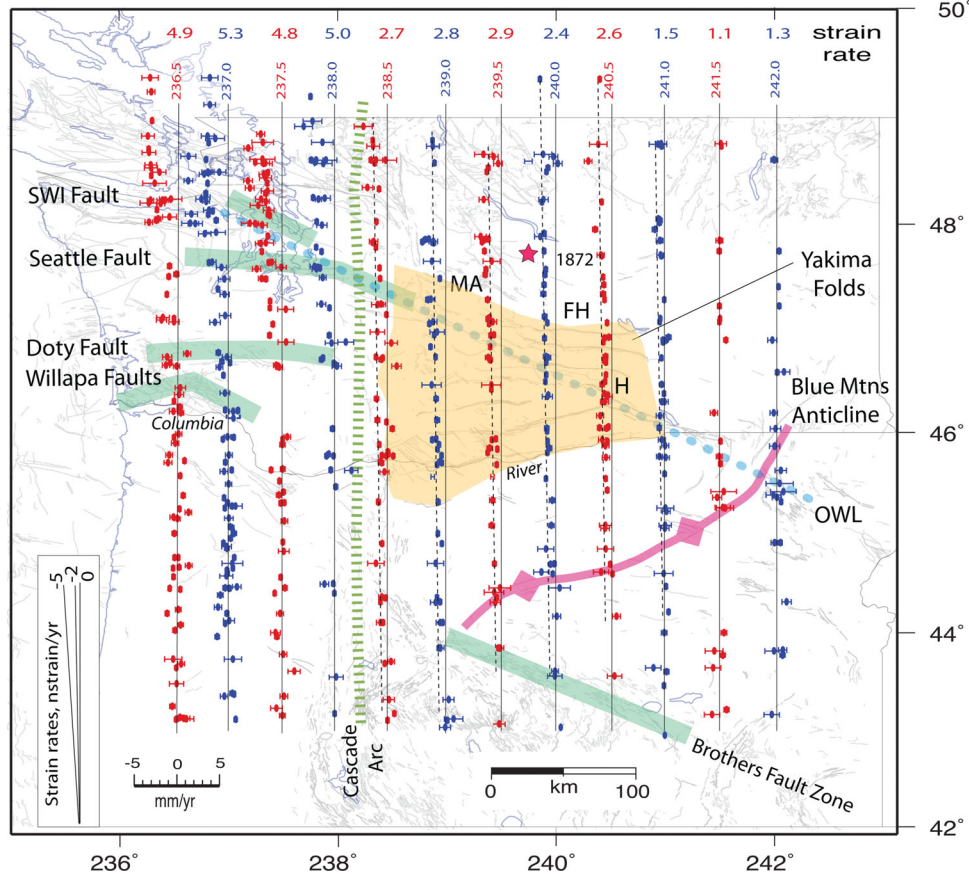


Figure 6. North–south profiles of the north components of GPS velocities overlain on fault map of Oregon and Washington (pale grey). Error bars for the velocities are $1-\sigma$. Longitude of each profile (alternating red and blue) and the average N–S strain rate in nstrain yr^{-1} (10^{-9} yr^{-1}) along the entire profile at top (formal uncertainties in strain rates range from 0.2 to 0.4 nstrain yr^{-1}). Fine dashed lines along profiles east of the arc are at a slope of $-2 \text{ nstrain yr}^{-1}$ for reference. Solid lines that provide baseline for velocities are aligned with the velocities at the south end of the profiles and are not zero (in North America reference frame). Orange shading outlines classical YFTB; strain extends beyond boundaries on north (FH: Frenchman Hills; MA: Manafort Anticline), south (Columbia River), and west (DF: Doty Hills fault; SF: Seattle fault; SWF: South Whidbey fault). H shows the location of Hanford, red star is the 1872 earthquake, blue dotted line is the location of Olympic-Wallowa Lineament (OWL), red bold line is the Blue Mountains Anticline; light green dashed line shows general location of Cascade volcanic arc.

shear occur along the arc and on the two N–S trending zones within the YFTB. Altogether this shear is no more than 1 mm yr^{-1} , with the greater part of the longitudinal gradient in the north velocity component being due to rotation.

5 DISCUSSION

Twenty years of GPS-derived surface velocities suggest that the current north–south shortening attributed to the YFTB occurs over a very large area from the BMA (44°N to 45°N) north to the border of the US with Canada. The total change in northward velocity between 43°N and 49°N on profiles east of the arc (238.2°E) and west of 241°E is about 2 to 3 mm yr^{-1} . This motion may have localization at the BMA (south of the CR) with a steady rate across the YFTB and north of the YFTB to about 49°N . The strain rates at the south boundary of the YFTB appear to be somewhat higher than within it and more localized, judging from the steeper velocity gradients. East of 242°E there is no observable change in the north component of velocity between 43°N and 49°N . West of the arc the change in northward velocity is 4 to 5 mm yr^{-1} and largely occurs north of the CR (46°N) on faults of the Puget Lowland region. The largest drops in the north velocity in the forearc appear to occur

near the Doty fault and the Seattle fault suggesting that shortening may be localized there.

Geologic data indicate that the current YFTB deformation revealed by GPS is occurring on structures that have a history of folding extending into the Eocene (~ 50 Ma; Walker & Robinson 1990; Haugerud & Tabor 2009). In the Blue Mountains, the folded CRBG (15–16 Ma) rests unconformably on folded 18–37 Ma tuffs and volcanioclastic strata of the John Day Formation, which itself is unconformable on more steeply dipping 37–50+ Ma andesites of the Clarno Formation (Fig. 1; Walker & Robinson 1990; Walker & MacLeod 1991). All of the Cenozoic units are unconformable on Cretaceous and older basement rocks, which are exposed in the cores of the anticlinal uplifts of the Blue Mountains (Fig. 1; Walker & Robinson 1990; Walker & MacLeod 1991). Both John Day ash flow tuffs and Columbia River Basalt flows lap onto the growing folds and are areally constrained by Blue Mountains structures (Hooper & Swanson 1990; Robinson *et al.* 1990). Similar CRBG relations have been documented for the central YFTB (Reidel 1984, 1989). Basement exposures along the western edge of the YFTB in the Washington Cascade Range demonstrate relations similar to the Blue Mountains, where Palaeogene volcanic and sedimentary rocks of the Cascade Range overlie highly deformed Mesozoic basement rocks and are themselves more tightly folded than the overlying

Columbia River Basalt (Haugerud & Tabor 2009). Pre-CRBG folding is inferred beneath the YFTB of Washington from gravity data, which shows pronounced, asymmetric gravity highs coincident with the anticlines, suggesting that the dense basement has topography similar to YFTB but higher in amplitude (Blakely *et al.* 2011).

The north–south zones of dextral shear and shortening in the YFTB, along longitudes 239.9°E and 240.9°E, coincide with the margins of a gravity high that trends north–south in the centre of the CRBG, which Saltus (1993) and Lamb *et al.* (2015) interpret to be the result of a broad basement high beneath the Columbia River basalts. They note that the western edge of the north–south basement high is traced at the surface by the Hog Ranch–Naneum Anticline in the CRBG, indicating reactivation of the structure in the late Cenozoic. The GPS velocities suggest the Hog Ranch–Naneum Anticline is a zone of active deformation today. The eastern zone of shortening at 240.9°E lies along the eastern margin of the gravity high, east of which is the Pasco Basin gravity low (Fig. 1; Blakely *et al.* 2014). This zone marks the easternmost edge of the most pronounced seismicity of the YFTB and the eastern termination of the YFTB faults, where they curve southward to align with the zone of shortening (Fig. 4c). The axis of this zone of shortening lies about 20 km east of and parallel to the eastern margin of the Hanford site and roughly parallels the 8.5 Ma Ice Harbor dike swarm (Reidel *et al.* 2013).

6 CONCLUSIONS

GPS velocities within and around the YFTB indicate a uniform strain rate of about 2 to 3 nstrain yr^{-1} across the YFTB with no clear localization at any particular faults, with the possible exception of the BMA. They reveal a much broader area of active shortening than anticipated. The deformation appears to start at the BMA in northern Oregon and extends northward through Washington to the Canadian border. The YFTB appears to be truncated at its eastern edge by an N–S zone of transpression near 240.9°E where seismicity and fault traces die off at the western edge of the Pasco Basin. East of 240.9°E, N–S gradients in velocities drop to about 1 nstrain yr^{-1} . A second N–S zone of geodetic transpression is found along the Hog Ranch–Naneum Anticline (~239.9°E) coincident with a strong gravity gradient and deflection of the YFTB fault traces. Together these two zones accommodate about 1 mm yr^{-1} of E–W shortening and 0.5 mm yr^{-1} of right-lateral shear and appear to arise from re-activation of basement structures.

ACKNOWLEDGEMENTS

Helping in the 2012–2014 field observations were Stan Liffmann, Ray Clayton, John Omer, Steve Reidel, Wade Holter and Sara, Emily, Hope and Jack McCaffrey. We thank the many landowners who allowed access to GPS marks. Wayne Thatcher, Mike Lisowski and Walter Szeliga contributed GPS observations. Helpful reviews were provided by Steve Reidel, Brian Sherrod, Takeshi Sagiyama and Zheng-Kang Shen. Continuous GPS data were obtained from SOPAC, UNAVCO, and PANGA/CWU archives. W. Szeliga provided metadata for the PANGA files. RM and RWK are supported by NEHRP grants G12AP20021 and G12AP20032, respectively. We acknowledge equipment services provided by the UNAVCO Facility with support from the National Science Foundation (NSF) and National Aeronautics and Space Administration (NASA) under NSF Cooperative Agreement No. EAR-0735156. All GPS field data and logsheets are archived at UNAVCO and

the velocity field is given in the Supporting Information. Strain rate calculations were done with TDEFNODE (McCaffrey 2009; web.pdx.edu/~mccaffr/defnode) and figures were drawn with GMT (Wessel & Smith 1998; www.soest.hawaii.edu/gmt).

REFERENCES

- Bakun, W.H., Haugerud, R.A., Hopper, M.G. & Ludwin, R.S., 2002. The December 1872 Washington State earthquake, *Bull. seism. Soc. Am.*, **92**, 3239–3258.
- Blakely, R.J., Sherrod, B.L., Weaver, C.S., Wells, R.E., Rohay, A.C., Barnett, E.A. & Kneprath, N.E., 2011. Connecting the Yakima fold and thrust belt to active faults in the Puget Lowland, Washington, *J. geophys. Res.*, **116**, B07105, doi:10.1029/2010JB008091.
- Blakely, R.J., Sherrod, B.L., Weaver, C.S., Wells, R.E. & Rohay, A.C., 2014. The Wallula fault and tectonic framework of south-central Washington, as interpreted from magnetic and gravity anomalies, *Tectonophysics*, **624**, 32–45.
- Campbell, N.D. & Bentley, R.D., 1981. Late Quaternary deformation of the Toppenish Ridge uplift in south-central Washington, *Geology*, **9**, 519–524.
- Gomberg, J., Sherrod, B., Trautman, M., Burns, E. & Snyder, D., 2012. Contemporary seismicity in and around the Yakima fold and thrust belt in eastern Washington, *Bull. seism. Soc. Am.*, **102**, 309–320.
- Haugerud, R.A. & Tabor, R.W., 2009. Geologic map of the North Cascade Range, Washington, in U.S. Geological Survey Scientific Investigations Map 2940, 2 sheets, scale 1:200,000, 2 pamphlets, 29 p. and 23 p.
- Herring, T.A., 2004. *GLOBK: Global Kalman Filter VLBI and GPS Analysis Program, Release 10.2*, Massachusetts Institute of Technology.
- Herring, T.A., King, R.W. & McCluskey, S.C., 2010. *Introduction GAMIT/GLOBK Release 10.4, November, 2010*, Massachusetts Institute of Technology.
- Hooper, P.R. & Swanson, D.A., 1990. The Columbia River Basalt Group and associated volcanic rocks of the Blue Mountains province, in *Geology of the Blue Mountains Region of Oregon, Idaho, and Washington: Cenozoic Geology of the Blue Mountains Region*, pp. 63–100, ed. Walker, G.W., U.S. Geological Survey, Professional Paper 1437.
- Kostrov, B.V., 1974. Seismic moment and energy of earthquakes, and seismic flow of rocks, *Izv. Earth Phys.*, **1**, 23–40.
- Ladinsky, T.C., Kelsey, H., Sherrod, B. & Pratt, T., 2010. Range-front deformation on the northern limb of the Manastash Anticline, Yakima fold belt, Washington, in *American Geophysical Union, Fall Meeting Abstract*, EP53B–0620.
- Lamb, A.P., Blakely, R.J., Wells, R.E., Sherrod, B.L. & Brocher, T.M., 2015. *Investigating Relationships Between the Yakima Fold and Thrust Belt and Basement Structure in Washington State Using Matched Filtering of Gravity and High-Resolution Aeromagnetic Data*, Society of Exploration Geophysicists, poster.
- Ludwin, R.S., Weaver, C.S. & Crosson, R.S., 1991. Seismicity of Washington and Oregon, in *Neotectonics of North America*, pp. 77–97, eds Slemmons, D.B., Engdahl, E.R., Zoback, M.D. & Blackwell, D.D., Geological Society of America.
- McCaffrey, R., 2009. Time-dependent inversion of three-component continuous GPS for steady and transient sources in northern Cascadia, *Geophys. Res. Lett.*, **36**, L07304, doi:10.1029/2008GL036784.
- McCaffrey, R., Long, M., Goldfinger, C., Zwick, P.C., Nabelek, J.L., Johnson, C.K. & Smith, C., 2000. Rotation and plate locking at the southern Cascadia subduction zone, *Geophys. Res. Lett.*, **27**, 2117–3120.
- McCaffrey, R. *et al.*, 2007. Fault locking, block rotation and crustal deformation in the Pacific Northwest, *Geophys. J. Int.*, **169**, 1315–1340.
- McCaffrey, R., King, R.W., Payne, S.J. & Lancaster, M., 2013. Active tectonics of Northwestern US inferred from GPS-derived surface velocities, *J. geophys. Res.*, **118**, doi:10.1029/2012JB009473.
- Pezzopane, S.K. & Weldon, R., 1993. Tectonic role of active faulting in central Oregon, *Tectonics*, **12**, 1140–1169.

- Pollitz, F.F., McCrory, P., Wilson, D., Svare, J., Puskas, C. & Smith, R.B., 2010. Viscoelastic-cycle model of interseismic deformation in the north-western United States, *Geophys. J. Int.*, **181**, 665–696.
- Pratt, T.L., 2012. Large-scale splay faults on a strike-slip fault system: the Yakima Folds, Washington State, *Geochem. Geophys. Geosyst.*, **13**, Q11004, doi:10.1029/2012GC004405.
- Puskas, C.M. & Smith, R.B., 2009. Intraplate deformation and microplate tectonics of the Yellowstone Hotspot and surrounding western U.S. interior, *J. geophys. Res.*, **114**, B04410, doi:10.1029/2008JB005940.
- Raisz, E., 1945. The Olympic-Wallowa Lineament, *Am. J. Sci.*, **243-A**, 479–485.
- Reidel, S., 1984. The Saddle Mountains: the evolution of an anticline in the Yakima fold belt, *Am. J. Sci.*, **284**, 942–977.
- Reidel, S.P., Fecht, K.R., Haggard, M.C. & Tolan, T.L., 1989. The geologic evolution of the central Columbia plateau, *Geol. Soc. Am. Spec. Paper*, **239**, 247–264 pp.
- Reidel, S.P., Campbell, N.D., Fecht, K.R. & Lindsey, K.A., 1994. Late Cenozoic structure and stratigraphy of south-central Washington: Wash. Div., *Geol. Earth Resour. Bull.*, **80**, 159–180.
- Reidel, S.P., Camp, V.E., Tolan, T.L., Kauffman, J.D. & Garwood, D.L., 2013. Tectonic evolution of the Columbia River flood basalt province, in *The Columbia River Flood Basalt Province*, pp. 293–324, eds Reidel, S.P., Camp, V.E., Ross, M.E., Wolff, J.A., Martin, B.S., Tolan, T.L. & Wells, R.E., Geological Society of America, Special Paper 497.
- Robinson, P.T., Walker, G.W. & McKee, E.H., 1990. Eocene (?), Oligocene, and lower Miocene rocks of the Blue Mountains region, in *Geology of the Blue Mountains Region of Oregon, Idaho, and Washington: Cenozoic Geology of the Blue Mountains Region*, pp. 29–61, ed. Walker, G.W., U.S. Geological Survey, Professional Paper 1437.
- Saltus, R.W., 1993. Upper-crustal structure beneath the Columbia River Basalt Group, Washington: gravity interpretation controlled by borehole and seismic studies, *Bull. geol. Soc. Am.*, **105**, 1247–1259.
- Savage, J.C., Lisowski, M. & Prescott, W.H., 1981. Geodetic strain measurements in Washington, *J. geophys. Res.*, **86**, 4929–4940.
- Savage, J.C., Lisowski, M. & Prescott, W.H., 1991. Strain accumulation in western Washington, *J. geophys. Res.*, **96**, 14 493–14 507.
- Sherrod, B.L., Blakely, R.J. & Weaver, C.S., 2015. LiDAR helps identify source of 1872 earthquake near Chelan, *EOS, Trans. Am. geophys. Un.*, **97**, Abstract T31A-2826.
- Walker, G.W. & Robinson, P.T., 1990. Cenozoic tectonism and volcanism of the Blue Mountains region, in *Geology of the Blue Mountains Region of Oregon, Idaho, and Washington: Cenozoic Geology of the Blue Mountains Region*, pp. 119–135, U.S. Geological Survey, Professional Paper 1437.
- Walker, G.W. & MacLeod, N.S., 1991. *Geologic Map of Oregon*, U.S. Geological Survey, scale 1:500 000.
- Waters, A.C., 1955. Geomorphology of south-central Washington, illustrated by the Yakima East quadrangle, *Bull. geol. Soc. Am.*, **66**, 633–684.
- Wells, R.E. & McCaffrey, R., 2013. Steady rotation of the Cascade arc, *Geology*, doi:10.1130/G34514.1.
- Wells, R.E., Weaver, C.S. & Blakely, R.J., 1998. Fore arc migration in Cascadia and its neotectonic significance, *Geology*, **26**, 759–762.
- Wessel, P. & Smith, W.H.F., 1998. New, improved version of the Generic Mapping Tools released, *EOS, Trans. Am. geophys. Un.*, **79**, 579.
- West, M.W., Ashland, F.X., Busacca, A.J., Berger, G.W. & Shaffer, M.E., 1996. Late Quaternary deformation, Saddle Mountains anticline, south-central Washington, *Geology*, **24**, 1123–1126.
- Wicks, C., Thelen, W., Weaver, C., Gomberg, J., Rohay, A. & Bodin, P., 2011. InSAR observations of aseismic slip associated with an earthquake swarm in the Columbia River flood basalts, *J. geophys. Res.*, **116**, B12304, doi:10.1029/2011JB008433.
- Yeats, R., 2011. *Active Faults of the World*, Cambridge Univ. Press.

SUPPORTING INFORMATION

Additional Supporting Information may be found in the online version of this paper:

Figure S1. Map of the Yakima fold and thrust belt of Washington and Oregon showing GPS site locations. Blue dots show locations of survey-mode GPS sites occupied by us in 2012 and 2013; green are new survey-mode sites established by us in 2012 and 2013; turquoise dots are continuous GPS sites of the PANGA and PBO (with triangle) networks that we have included; and red dots are other survey-mode sites that we did not re-occupy.

Figure S2. (A) Map of eastern Oregon, eastern Washington and western Idaho showing residuals after removing rotation and uniform strain from Blocks 2 and 3 and rotation only from Block 1. We estimated three rotation poles and two uniform horizontal strain rate tensors (15 total parameters) using the 160 sites (320 observations) that have velocity uncertainties less than 0.8 mm yr^{-1} . A minimum uncertainty of 0.2 mm yr^{-1} is applied to any less than this. Green arrows show principal strain rates and rotation poles are blue ellipses with rates given in deg Ma^{-1} . Error ellipses on velocities are 70 per cent. (B,C) Distribution of normalized residuals (histogram) for east and north components of velocities compared to theoretical curve for Gaussian distribution (smooth curve).

Figure S3. East components of selected continuous GPS time-series showing SSE and their possible extension into the Yakima region. Sites are arranged from west at top to east at bottom. The YFTB extends from about P065 (239.0E) to P451 (241.0E). The 2011 SSE, a westward deflection, is evident as far east as P452 (240.5E).

Figure S4. Locking distributions used to estimate elastic strain rates across the YFTB. (A) Locking is constrained to be a Gaussian function of depth. (B) Locking is estimated at rectangular patches along the plate interface. Red dots show GPS locations where only horizontal velocities are used; blue dots show where vertical rates were used either from GPS or levelling. Triangles are locations of volcanoes. See McCaffrey *et al.* (2013) for details.

Figure S5. Surface strain rates estimated from GPS velocity field. Top shows east–west strain rate and bottom shows north–south strain rate ($\text{nstrain} = 10^{-9}$). Red dots show grid points. Blue colours indicate contraction and yellow–red indicate extension. Note that the strain rate scale is a factor of 10 larger for E–W than it is for N–S.

Figure S6. South-to-north profiles of the north component (black dot) of the GPS velocities at each 0.5° of longitude from 236.5E to 242.0E (longitude given in plot). Error bars are $1-\sigma$. Green curve is the topography using scale at left. Red curve is predicted north velocity from fitting of strain rate map in Supporting Information Fig. S5. In panels 236.5 to 238.0 blue dashed lines are at slopes of 0 ns yr^{-1} ($=10^{-9} \text{ per year}$) on left (south) side and sloping in the north as labelled. For remaining panels slope is constant for entire profile, as labelled. At the bottom is the latitude along the profiles. Note the change in the mm yr^{-1} scale between the first four profiles (west of arc) and the last eight (east of arc).

Table S1. GPS Velocities relative to North America with $1-\sigma$ uncertainties.

(<http://gji.oxfordjournals.org/lookup/suppl/doi:10.1093/gji/ggw252/-DC1>).